



HAL
open science

Correlation between negative magnetoresistance effect and magnon excitations in single-crystalline $\text{CuCr}_{1.6}\text{V}_{0.4}\text{Se}_4$

Ewa Malicka, Tadeusz Groń, Danuta Skrzypek, Andrzej W. Pacyna, Dariusz Badurski, Alicja Waśkowska, Sławomir Mazur, Rafał Sitko

► **To cite this version:**

Ewa Malicka, Tadeusz Groń, Danuta Skrzypek, Andrzej W. Pacyna, Dariusz Badurski, et al.. Correlation between negative magnetoresistance effect and magnon excitations in single-crystalline $\text{CuCr}_{1.6}\text{V}_{0.4}\text{Se}_4$. Philosophical Magazine, 2010, 90 (11), pp.1525-1541. 10.1080/14786430903405504 . hal-00584287

HAL Id: hal-00584287

<https://hal.science/hal-00584287>

Submitted on 8 Apr 2011

HAL is a multi-disciplinary open access archive for the deposit and dissemination of scientific research documents, whether they are published or not. The documents may come from teaching and research institutions in France or abroad, or from public or private research centers.

L'archive ouverte pluridisciplinaire **HAL**, est destinée au dépôt et à la diffusion de documents scientifiques de niveau recherche, publiés ou non, émanant des établissements d'enseignement et de recherche français ou étrangers, des laboratoires publics ou privés.



Correlation between negative magnetoresistance effect and magnon excitations in single-crystalline $\text{CuCr}_{1.6}\text{V}_{0.4}\text{Se}_4$

| | |
|-------------------------------|--|
| Journal: | <i>Philosophical Magazine & Philosophical Magazine Letters</i> |
| Manuscript ID: | TPHM-09-Jul-0306 |
| Journal Selection: | Philosophical Magazine |
| Date Submitted by the Author: | 20-Jul-2009 |
| Complete List of Authors: | Malicka, Ewa; University of Silesia, Institute of Chemistry Groń, Tadeusz; University of Silesia, Institute of Physics Skrzypek, Danuta; University of Silesia, Institute of Physics Pacyna, Andrzej; Polish Academy of Sciences, The Henryk Niewodniczański Institute of Nuclear Physics Badurski, Dariusz; Polish Academy of Sciences, Institute of Low Temperatures and Structure Research Waśkowska, Alicja; Polish Academy of Sciences, Institute of Low Temperatures and Structure Research Mazur, Sławomir; University of Silesia, Institute of Physics Sitko, Rafał; University of Silesia, Institute of Chemistry |
| Keywords: | electron paramagnetic resonance, magnetoresistance, spinels, thermoelectric power |
| Keywords (user supplied): | magnetoresistance, spin waves, thermoelectric effects |
| | |



1
2
3
4
5
6
7
8
9
10
11
12
13
14
15
16
17
18
19
20
21
22
23
24
25
26
27
28
29
30
31
32
33
34
35
36
37
38
39
40
41
42
43
44
45
46
47
48
49
50
51
52
53
54
55
56
57
58
59
60

Correlation between negative magnetoresistance effect and magnon excitations in single-crystalline $\text{CuCr}_{1.6}\text{V}_{0.4}\text{Se}_4$

E. Malicka,¹ T. Groń,² D. Skrzypek,² A.W. Pacyna,³ D. Badurski,⁴

A. Waśkowska,⁴ S. Mazur,² and R. Sitko¹

¹*University of Silesia, Institute of Chemistry, ul. Szkolna 9, 40-006 Katowice, Poland*

²*University of Silesia, Institute of Physics, ul. Uniwersytecka 4, 40-007 Katowice, Poland*

³*The Henryk Niewodniczański Institute of Nuclear Physics, Polish Academy of Sciences, ul. Radzikowskiego 152, 31-342 Kraków, Poland*

⁴*Institute of Low Temperature and Structure Research, Polish Academy of Sciences, ul. Okólna 2, 50-950 Wrocław, Poland*

The structural, electrical and magnetic measurements as well as the electron spin resonance (ESR) spectra were used to characterize the single-crystalline $\text{CuCr}_{1.6}\text{V}_{0.4}\text{Se}_4$ spinel and to study a correlation between negative magnetoresistance effect and magnon excitations. The ferromagnetic order below the Curie temperature $T_C \approx 193$ K, a p -type semiconducting behavior, the ESR change from paramagnetic to ferromagnetic resonance at T_C , a big value of ESR linewidth and its temperature dependence in paramagnetic region were established. The electrical studies revealed the negative magnetoresistance, which can be enhanced with increasing magnetic field and decreasing temperature while a detailed thermopower analysis showed the magnon excitations at low temperatures. The spin-phonon coupling is explained within a

1 framework of the complex model of paramagnetic relaxation processes as the
2
3 several-stage relaxation process in which the V^{3+} ions, the exchange subsystem
4
5 and conduction electrons subsystem act as the intermediate reservoirs.
6
7
8
9

10
11
12 Keywords: magnetoresistance; spin waves; thermoelectric effects; electron spin
13
14 resonance
15

16 17 18 19 20 21 **1. Introduction** 22 23 24 25

26 Kanamori [1] predicted that 90° ferromagnetic (FM) superexchange occurs
27
28 between octahedrally coordinated $3d^3$ ions. For example, in the p -type FM
29
30 semiconductor $CdCr_2Se_4$ with the Curie temperature $T_C = 142$ K and the Curie-
31
32 Weiss (CW) temperature $\theta_{CW} = 190$ K the FM superexchange occurs within the
33
34 Cr sublattice *via* the 90° Cr-Se-Cr σ/π bonding which links a half-filled $t_{2g}(\pi)$
35
36 orbital of one of Cr-ions with an empty $e_g(\sigma)$ level on the other Cr [2,3]. In the
37
38 parent FM $CuCr_2Se_4$ being a p -type metallic conductor with $T_C = 416$ K and θ_{CW}
39
40 = 436 K [4], the chromium spins are coupled ferromagnetically *via* double
41
42 exchange interaction involving the electrons jumping between Cr^{3+} and Cr^{4+} ions
43
44 [5,6]. The X-ray photoelectron spectroscopy and polarized neutron diffraction
45
46 study for $CuCr_2Se_4$ provided a direct evidence for the presence of monovalent
47
48 copper atoms with a $3d^{10}$ configuration [7,8]. However, it was not possible to
49
50 measure in $CuCr_2Se_4$ the magnetic splitting of the Cr $3s$ levels, because these
51
52 levels overlapped with the Cu $3p$ ones [7]. The second end composition of the
53
54
55
56
57
58
59
60

1 CuCr_{2-x}V_xSe₄ system, *i.e* CuV₂Se₄ is not known, yet. In the isostructural CuCr₂₋
2
3
4 _xV_xS₄ spinel system a rapid decrease of T_C from 267 K for $x = 0.25$ to 8 K for x
5
6 = 1.75 was observed [9]. This fact has been explained by being weaker Cr-S-V
7
8 superexchange interactions than the original Cr-S-Cr ones as well by a
9
10 weakening of the nearest neighbor ferromagnetic Cr-S-Cr interactions due to the
11
12 initial lattice expansion [9].
13
14

15
16
17 Recently, numerous efforts have been made to find a correlation between
18
19 the thermoelectric power and the double exchange and superexchange
20
21 interactions in the CdCr_{2-x}Ga_xSe₄, Zn_xCu_yCr_zSe₄, Cu_xGa_yCr_zSe₄ and
22
23 Cu_xCo_yCr_zSe₄ spinel series [10-14]. These studies have shown that the strong
24
25 ferromagnetic coupling connected mainly with the double-exchange mechanism,
26
27 makes easier both the magnon excitations and a transfer of the phonon
28
29 momentum to the electron gas. The opposite behavior for the ferrimagnetic and
30
31 antiferromagnetic spin arrangements was observed.
32
33
34
35
36
37

38
39 It seems thus natural to expect a coupling between the magnon and electron
40
41 systems leading to the negative magnetoresistance effect in single-crystalline
42
43 CuCr_{1.6}V_{0.4}Se₄ spinel. For that the Bloembergen and Wang model of
44
45 paramagnetic relaxation processes [15], the high-temperature expansion of the
46
47 magnetic susceptibility and the thermoelectric power analysis were used.
48
49
50
51
52
53

54 55 56 **2. Experiment**

57 58 *2.1. Preparation*

59
60 The single crystal of CuCr_{1.6}V_{0.4}Se₄ spinel was obtained by the chemical

1 vapour transport method [16] in a closed quartz ampoule containing binary
2
3 selenide CuSe, and stoichiometric amounts of high purity (99.99%) elements:
4
5 vanadium and selenium. Anhydrous chromium chloride CrCl₃ was used as the
6
7 chemical transport agent. The ampoule was heated in a horizontal zone furnace
8
9 for four weeks. The temperature of the solution and crystallization zone was
10
11 1273 K and 1223 K, respectively. The resulting single crystal was of octahedral
12
13 shape with regular {111} faces, the edge length being 4 mm.
14
15
16
17
18

19
20 For the crystal structure characterization, describing the cation distribution
21
22 over the tetrahedral and octahedral sites formed by the selenium sublattice, a
23
24 good quality sample was selected for the intensity data collection with a single
25
26 crystal X-ray diffraction technique. The intensities were measured with a KM-
27
28 4/CCD (Oxford Diffraction) instrument, operating in κ geometry and using
29
30 graphite monochromated MoK α radiation ($\lambda=0.71073$ Å). The ω -scan technique
31
32 was used for data collection. Integration of the intensity data and corrections for
33
34 Lorentz – polarization effects and absorption were made using *CrysAlis* software
35
36 [17]. The absorption correction was applied with the Gaussian face-indexed
37
38 numerical routine [18]. The structure calculations were performed using the
39
40 SHELXL-97 program system [18].
41
42
43
44
45
46
47
48
49

50
51 The chemical composition of the CuCr_{1.6}V_{0.4}Se₄ single crystal was
52
53 determined by the energy-dispersive X-ray spectrometry (EDXRF). The sample
54
55 was excited by the air-cooled side-window Rh target X-ray tube of 125 μ m
56
57 thickness Be window and ca. 100 μ m nominal focal spot size (XTF 5011/75,
58
59 Oxford Instruments, USA). The X-ray tube was supplied with the XLG high-
60

1 voltage generator (Spellman, USA). The tungsten pinhole collimator was used to
2
3 reduce the size of analyzed area. For the collimators of the size holes of 100,
4
5 200, 400, 1000 and 2000 μm , the following focal spot sizes are obtained: 169,
6
7 280, 581, 1469, 2888 μm . The X-ray spectra of the samples were collected by
8
9 thermoelectrically cooled Si-PIN detector (XR-100CR Amptek, Bedford, MA,
10
11 USA) of 6 mm^2 active area, 500 μm crystal thickness and 12.5 μm Be window
12
13 thickness. The Si-PIN detector cooled to the temperature of ca. -55°C reaches
14
15 the resolution of 145 eV at 5.9 keV. The Si-PIN detector was coupled to a
16
17 multichannel analyzer (PX4 Amptek, Bedford, MA, USA). In the constructed
18
19 spectrometer, the incidence and take-off angles were 45° . The position of the
20
21 sample was moved using the X-Y stage and was monitored by CCD camera and
22
23 two laser pointers. The weight composition of the single crystal under study is as
24
25 follows: Cu – 13.1 ± 0.2 , Cr – 17.3 ± 0.3 , V – 4.26 ± 0.08 , Se – 65.4 ± 0.8 .
26
27 These values have been converted into percent of the atomic content.
28
29
30
31
32
33
34
35
36
37
38
39
40
41
42

43 2.2. *Electrical and magnetic measurements*

44
45
46 The mass magnetization was measured at 4.6 K and in external magnetic
47
48 fields up to 60 kOe while the static (dc) mass susceptibility measurements were
49
50 performed in the temperature range 4.2-350 K and in applied external magnetic
51
52 field of 900 Oe using a Faraday type Cahn RG automatic electrobalance.
53
54
55

56
57 The electrical measurements have been done in the temperature range 7-
58
59 300 K. The electrical resistivity ρ has been measured with the 4-point dc method
60
using the apparatus with Keithley K181 digital multimeters. The maximal error

1 $\delta\rho/\rho$ was less than ± 1 %. The magnetoresistance measurements were performed
2
3
4 in the magnetic fields up to 8 T at 4.3, 10, 15, 20 and 40 K and at fixed magnetic
5
6 field 8 T in the temperature range 7-110 K. The direction of magnetic field was
7
8 perpendicular to the current sample. The thermoelectric power was measured
9
10 with a differential method using the temperature gradient ΔT of about 2 K. The
11
12 accuracy of the value of thermopower was estimated to be better than 3 $\mu\text{V/K}$.
13
14 The electrical and thermal contacts between the single crystal and the copper
15
16 rods were maintained with a silver lacquer mixture (Degussa Leitsilber 200).
17
18 The thermoelectric power and the electrical resistivity of the same sample were
19
20 measured along the $\langle 001 \rangle$ direction. The crystal orientation about the $\langle 001 \rangle$
21
22 crystallographic zone axis, was based on 12-18 centered X-ray diffraction
23
24 reflections with the Bragg angles in the range $107 \leq 2\theta \leq 144^\circ$ (MoK α
25
26 radiation). The checking electrical measurements in the $\langle 111 \rangle$ direction,
27
28 performed for comparison, showed unimportant difference with those along
29
30 $\langle 001 \rangle$.
31
32
33
34
35
36
37
38
39
40
41
42
43
44
45

46 2.3. ESR measurements

47
48 The electron spin resonance (ESR) spectra were measured in the
49
50 temperature range 77-275 K using a 100-kHz field-modulated spectrometer
51
52 operated at 9 GHz, so that the derivatives of the absorption signals were
53
54 recorded. A continuous nitrogen flow cryostat was used to study temperature
55
56 dependence. For ESR measurements the obtained crystals were crushed into
57
58 powder and diluted in the paraffin to reduce the skin effect. The shape and area
59
60

of the ESR spectra were analyzed by numerical method.

3. Results

3.1. Crystallographic properties

Crystal data, experimental details and structure refinement results for the single-crystal of $\text{CuCr}_{1.6}\text{V}_{0.4}\text{Se}_4$ spinel are collected in Table 1. They are showing that the compound crystallizes in a cubic structure with space group $Fd\bar{3}m$ (#227) and the unit cell of dimension $a = 1034.99(12)$ pm, being slightly elongated in comparison with $a = 1033.5(3)$ pm of the parent CuCr_2Se_4 [6]. The structure model with the diamagnetic Cu ions occupying the tetrahedral $8a$ positions and the magnetic Cr and V-ions sharing the octahedral $16d$ sites, converged satisfactorily. The site occupancy factors treated as free variables in the least-squares structure refinement, confirmed the sample composition and the cation distribution according to the spinel formula: $\text{Cu}[\text{Cr}_{1.6}\text{V}_{0.4}]\text{Se}_4$.

3.2. Electrical and magnetic properties

The electrical resistivity $\rho(T)$ and thermoelectric power $S(T)$ measurements depicted in Fig. 1 reveal a p -type semiconducting behaviour of the $\text{CuCr}_{1.6}\text{V}_{0.4}\text{Se}_4$ single crystal. The values of $\rho(T)$ and $S(T)$ are close to those for CuCr_2Se_4 [19]. The variation of $\rho(T)$ does not follow a simple exponential behaviour, because a gradual decrease of resistivity and strong slope at T_C with increasing temperature are observed. The $S(T)$ shows a broad hump at 100 K and reaches a minimum at T_C from one side and goes to (0, 0) from the other.

1 The $\rho(T)$ dependence decreases with increasing magnetic field, revealing the
 2
 3 negative magnetoresistance effect shown in Fig. 2. Moreover, the lower
 4
 5 temperature, the larger negative magnetoresistance, $\Delta\rho/\rho_0(H)$. However, in the
 6
 7 temperature range 10-20 K the negative values of $\Delta\rho/\rho_0(H)$ increase
 8
 9 insignificantly as temperature decreases (Fig. 2).
 10
 11
 12
 13

14 The results of the magnetic measurements are depicted in Figs. 3 and 4.
 15
 16 The dc mass susceptibility vs. temperature, $\chi_\sigma(T)$, shows a ferromagnetic order
 17
 18 with the Curie temperature $T_C = 193.2$ K. Above 200 K, $\chi_\sigma^{-1}(T)$ follows the CW
 19
 20 behavior with a positive CW temperature $\theta_{CW} = 207$ K and an effective moment
 21
 22 $\mu_{eff} = 2.83\sqrt{MC_\sigma} = 5.85 \mu_B/\text{f.u.}$, where the molar mass $M \approx 482.96$ g/mol and
 23
 24 the Curie constant $C_\sigma = 8.873 \cdot 10^{-3}$ K·cm³/g. This value is somewhat higher than
 25
 26 the spin-only value of $5.22 \mu_B/\text{f.u.}$ for $3d^3$ Cr³⁺ and $3d^2$ V³⁺ ions as well as of
 27
 28 $5.50 \mu_B/\text{f.u.}$ for $3d^9$ Cu²⁺, $3d^3$ Cr³⁺ and $3d^2$ V³⁺ ions. It means that the chromium
 29
 30 ions may form a mixed valence band. In Fig. 4 a shape of magnetic isotherm,
 31
 32 $\sigma(H)$, measured up to 60 kOe and at 4.6 K exhibits a saturation magnetization of
 33
 34 53.84 Oe·cm³/g ($4.66 \mu_B$) at 4 kOe already. In the inset of Fig. 4 a linear increase
 35
 36 of magnetization with increasing magnetic field, indicates a lack of spontaneous
 37
 38 magnetization below 4 kOe.
 39
 40
 41
 42
 43
 44
 45
 46
 47
 48
 49
 50
 51
 52
 53
 54
 55

56 3.3. ESR spectra

57
 58 The resonance spectra for CuCr_{1.6}V_{0.4}Se₄ consist of a single line in the
 59
 60 range from room temperature to $T_1 = 200$ K. At room temperature the intensity

1 of the resonance line is very weak. Below T_1 the spectra were simulated with
2
3
4 two profiles. The Figures 5(a), (b) and (c) show the temperature dependence of
5
6 the ESR parameters: ΔB - linewidth, B_r - resonance field and DI - intensity of
7
8 the spectrum. The corresponding values of the ΔB and B_r were obtained as the
9
10 fitting parameters and the DI values were calculated as double integration of the
11
12 spectrum. Starting from the $T = 272$ K ($\Delta B = 159.2$ mT) the linewidth values
13
14 rapidly decrease as the temperature is lowered to T_1 where $\Delta B = 27.8$ mT. Next,
15
16 the linewidth passes through a minimum and with decreasing temperature shows
17
18 a continuous broadening. The line-shape analysis shows that the ESR line
19
20 remains Lorentzian down to $T = 212$ K, and below this temperature a deviation
21
22 towards an asymmetrical line occurs. The shift of the resonance field (B_r) from
23
24 the high temperature value is observed below $T = 212$ K. In the temperature
25
26 range from $T = 193$ K to $T = 85$ K this effect is very significant. In Fig. 5(c) the
27
28 temperature evolution of the intensity of the ESR spectrum is shown with the
29
30 values reduced to $T = 272$ K. In the temperature range from $T = 225$ K to $T =$
31
32 183 K, the intensity rapidly increases. The intensity of ESR spectrum defined as
33
34 DI (double integration of the spectrum) should be proportional to the spin
35
36 susceptibility of the sample. The Curie temperature estimated from the $DI(T)$
37
38 dependence equals 193.8 K. The agreement with the susceptibility
39
40 measurements is satisfactory thus the ESR data appear to be consistent with the
41
42 magnetic ones.
43
44
45
46
47
48
49
50
51
52
53
54
55
56
57
58
59
60

4. Discussion

An explanation of the negative magnetoresistance effect in single-crystalline $\text{CuCr}_{1.6}\text{V}_{0.4}\text{Se}_4$ spinel is considered within a framework of spin-spin and spin-phonon couplings and also as a coupling between magnon and electron systems. For that a complex model of the paramagnetic relaxation processes and the thermoelectric power analysis are discussed in detail.

4.1. ESR studies

The linewidth value of $\text{CuCr}_{1.6}\text{V}_{0.4}\text{Se}_4$ at room temperature is about 200 mT. To understand the origin of the observed linewidth we have to estimate the relaxation contributions of the relevant spin-spin and spin-phonon interactions. In the chromium spinels, the Cr^{3+} ions always occupy the B-site of the spinel structure. The local symmetry at the octahedral site leads to the nondegenerate orbital ground state with $S = 3/2$. On the other hand, for the $3d^2$ configuration of V^{3+} ($S = 1$), the 3F free ion ground state is split by the octahedral field leaving an orbital triplet (T_2) lowest. Because of that, Cr^{3+} is the ion weakly coupled to the lattice in comparison with the fast-relaxing V^{3+} ions [19].

The ESR linewidth, ΔB , is related to the relaxation of the spin system. For individual spins $\Delta B \sim 1/\tau$, where τ is the spin relaxation time. In a dense magnetic material, this relationship is modified since the magnetization relaxes towards an effective field instead of the external field. In the examined compound it can be expected that the presence of V^{3+} ions essentially changes the resonance linewidth. In paramagnetic state (PM) (*i.e.* for $T > 212$ K) the

1 linewidth can be described by the following expression:
 2
 3
 4
 5

$$6 \Delta B = \Delta B_{ss} + \Delta B_{s-ph} \quad (1)$$

7
 8
 9
 10
 11 where ΔB_{ss} is described by the exchange narrowing theory [20]:
 12
 13
 14

$$15 \Delta B_{ss} = [(\Delta B_{dd})^2] / B_{ex}, \quad (2)$$

16
 17
 18
 19
 20
 21
 22
 23
 24
 25
 26
 27
 28
 29
 30
 31
 32
 33
 34
 35
 36
 37
 38
 39
 40
 41
 42
 43
 44
 45
 46
 47
 48
 49
 50
 51
 52
 53
 54
 55
 56
 57
 58
 59
 60
 (i.e. is proportional to the square of the dipolar produced linewidth ΔB_{dd} divided by the rate of exchange B_{ex}) and ΔB_{s-ph} represents the contributions of the spin-phonon interaction.

The complex model of paramagnetic relaxation processes, illustrated in Fig. 6, can be derived by analogy with the model of Bloembergen and Wang [15,21]. The Zeeman subsystem contains Cr^{3+} and V^{3+} ions and the vanadium is directly coupled to the lattice. The exchange subsystem includes the exchange-coupled Cr-Cr, Cr-V, V-V pairs. In the parent $CuCr_2Se_4$ spinel, which is a well studied metallic ferromagnet with $T_C = 416$ K [4], the high value of T_C is related to the exchange through the current of the hole carriers [5,6] including also the subsystem of conduction electrons. That model explains also a big ESR linewidth for $CuCr_{1.6}V_{0.4}Se_4$ and its temperature dependence in the PM state (Fig. 5(a)). The parameter of the thermal broadening linewidth $b = d(\Delta B)/dT = 1.9$ mT/K is rather high and means a fast energy flow from the spin subsystem to the $CuCr_{1.6}V_{0.4}Se_4$ lattice [22]. We suppose that the process of spin-lattice

1 relaxation includes both the interaction between the conduction electron spins
 2 and magnetic spins (Korringa effect) and also the vibrational modulation of
 3 exchange interactions. According to the Huber's and Seehra's theory for
 4 magnetically concentrated systems [23,24], the relationship between
 5 temperature and resonance linewidth can be explained by the Korringa
 6 mechanism [22] and spin-phonon relaxation processes in which are participating
 7 broad bands of phonons.
 8
 9
 10
 11
 12
 13
 14
 15
 16
 17
 18

19
 20 The temperature dependence of ΔB and B_r in the temperature range 212 –
 21 193 K (Fig. 5(a) and (b)) indicates that the magnetic short-range order develops.
 22 In this case, the spin correlations act as an effective internal field and therefore
 23 cause a shift of the resonance field B_r from that at high temperatures, where no
 24 magnetic short-range order exists. Simultaneously, the linewidth ΔB as $T \rightarrow T_C$
 25 from the high temperature side can be written as follows:
 26
 27
 28
 29
 30
 31
 32
 33
 34
 35
 36
 37
 38
 39

$$40 \Delta B = \Delta B_{\text{noncrit}}(T) + \Delta B_{\text{crit}}(T), \quad (3)$$

41
 42
 43
 44
 45 where: $\Delta B_{\text{noncrit}}$ and ΔB_{crit} factors represent the noncritical and critical
 46 contributions to the linewidth, respectively, and $\Delta B_{\text{noncrit}}$ is given by Eq. (1). The
 47 growth of linewidth (ΔB_{crit}) reflects the increase in the lifetime and the
 48 correlation length of the critical fluctuations. The appearance of the short-range
 49 magnetic ordering is confirmed by the temperature dependence of the spectrum
 50 intensity (Fig. 5(c)). As the temperature is reduced from about $T = 225$ K, the
 51 values for intensity rapidly increase. The ferromagnetic ordering temperature T_C
 52
 53
 54
 55
 56
 57
 58
 59
 60

1 = 193.8 K can be inferred from the location of coincident anomalies in the ESR
2
3
4 data: ΔB , B_r , DI (Fig. 5). The ESR spectrum of $\text{CuCr}_{1.6}\text{V}_{0.4}\text{Se}_4$ observed below T
5
6 = 193 K undergoes qualitative changes and transforms from paramagnetic (EPR)
7
8 into ferromagnetic (FMR) resonance. At low temperatures the experimental
9
10 spectrum was fitted by two profiles shown in Fig. 5(a) and (b). It is known, that
11
12 FMR can be adequately described in terms of the Landau-Lifshitz-Gilbert
13
14 equation [25] for the effective internal magnetic fields, which are attributed to
15
16 demagnetization and magnetocrystalline anisotropy fields. However, as in our
17
18 resonance measurements the sample in powdered form was examined, the shape
19
20 of FMR spectrum is the envelop of several components. As can be seen from
21
22 Fig. 5(a) and (b), the position and linewidth of this spectrum depends
23
24 monotonously on the temperature.
25
26
27
28
29
30
31
32
33
34
35
36

37 4.2. Thermoelectric power analysis

38
39 In this section we consider a coupling between the magnon and electron
40
41 systems based on the thermoelectric power analysis. Generally, in the magnetic
42
43 materials the magnetic component of thermopower (MCTP) may result from a
44
45 coupling of the phonon system to the electron gas via the spin lattice (magnon
46
47 gas), which is known as the Kasuya model [26], or from the transfer of the
48
49 magnon momentum to the electron gas (magnon drag) [27]. This magnetic
50
51 contribution is described by the Bloch law [28], *i.e.* the spontaneous
52
53 magnetization decreases with temperature at $T^{3/2}$ when T is small [29].
54
55 Analogous temperature dependence of MCTP has been directly derived from a
56
57
58
59
60

1 theoretical model of magnon-assisted transport in a mesoscopic tunnel junction
 2
 3 between a ferromagnetic metal and a normal (nonmagnetic) metal [30] for a
 4
 5 magnetic component of thermoelectric power.
 6
 7

8
 9 The experimental curve shape of thermopower $S(T)$ of the spinel single
 10
 11 crystal under study (Fig. 1) can be easily fitted by the modified Matoba, Anzai
 12
 13 and Fujimori semiempirical formula [31] including the magnetic contribution
 14
 15 [13] as follows:
 16
 17

$$18 \quad S(T) = D \cdot T + E \cdot T^3 + \frac{F \cdot \left(\frac{T}{\theta_D}\right)^3}{G + \left(\frac{T}{\theta_D}\right)^4} + H \cdot T^{1/2} + \frac{I \cdot \left(\frac{T}{J_{eff}^{aa}}\right)^{3/2}}{K + \left(\frac{T}{J_{eff}^{aa}}\right)^{5/2}} \quad (4)$$

19
 20 where θ_D is the Debye temperature (see Appendix A), and J_{eff}^{aa} is the effective
 21
 22 exchange integral for the first coordination sphere (see Appendix B). First and
 23
 24 second terms in Eq. (4) is the diffusion component where the small correction E
 25
 26 is the temperature dependence of D [32], third term in Eq. (4) is the phonon drag
 27
 28 component, fourth term in Eq. (4) is the impurity component, and the last term
 29
 30 in Eq. (4) is the magnon drag component. D , E , F , G , H , I and K in Eq. (4) (listed
 31
 32 in Table II) are the curve-fitting parameters. The agreement index R between the
 33
 34 experimental (S_{exp}) and the theoretical (S_{theor}) thermopowers is high (over 99 %,
 35
 36 see Table 2).
 37
 38
 39
 40
 41
 42
 43
 44
 45
 46
 47
 48
 49

50
 51 The results of thermopower analysis of the single-crystalline $\text{CuCr}_{1.6}\text{V}_{0.4}\text{Se}_4$
 52
 53 depicted in Fig. 7 show that the intensity of the magnon drag component (S_{mag})
 54
 55 is the largest and reaches a maximum of 7.86 $\mu\text{V/K}$ at 33 K. It means that the
 56
 57 magnon excitations, usually driven by the double exchange mechanism, are
 58
 59 observed only at low temperatures, and the maximum transfer of the magnon
 60

1 momentum to the electron gas may be a main reason for the observed the
 2 negative magnetoresistance effect. This effect disappears at higher temperatures.
 3
 4 The contribution to the total thermopower originates then mainly from the
 5
 6 phonon component (S_{ph}) which reveals a maximum of $7.1 \mu\text{V/K}$ at 100 K, *i.e.*
 7
 8 exactly in the theoretical temperature range $\theta_{\text{D}}/10 - \theta_{\text{D}}/2$ predicted by the Debye
 9
 10 theory [27], where in our case $\theta_{\text{D}} = 279.7 \text{ K}$ (see Table 2). At high temperatures
 11
 12 the diffusion component (S_{diff}) dominates, and according to the Mott formula
 13
 14 [33] it is proportional to temperature. The $S_{\text{diff}} = 5.6 \mu\text{V/K}$ at 300 K. The so-
 15
 16 called impurity component of the thermopower (S_{imp}) described by the $T^{1/2}$ law
 17
 18 [34] generates a maximum $1.51 \mu\text{V/K}$ at 300 K.

29 From the results of the magnetic considerations presented in Table 3 (see
 30 Appendix B) it follows that with increasing vanadium content x : (1) contribution
 31
 32 of the superexchange interaction to the Curie-Weiss temperature θ_{CW} suddenly
 33
 34 increases from 90 K for CuCr_2Se_4 to 163 K for $\text{CuCr}_{1.6}\text{V}_{0.4}\text{Se}_4$, (2) contribution
 35
 36 of the double exchange interaction to the Curie-Weiss temperature θ_{CW} and the
 37
 38 total hopping integral B rapidly decrease, and (3) the W_d bandwidth of the $3d t_{2g}$
 39
 40 band due to Cr^{3+} and Cr^{4+} ions decreases from 0.76 eV for CuCr_2Se_4 to 0.11 eV
 41
 42 for $\text{CuCr}_{1.6}\text{V}_{0.4}\text{Se}_4$. In the studied single crystal the superexchange J_{aa} and J_{ab}
 43
 44 integrals for the first two coordination spheres are positive and negative,
 45
 46 respectively, the absolute value of J_{aa} is over nine times larger than J_{ab} , the
 47
 48 double exchange b_{aa} and b_{ab} integrals for the first two coordination spheres are
 49
 50 positive and b_{aa} is five times larger than b_{ab} , and the effective exchange
 51
 52
 53
 54
 55
 56
 57
 58
 59
 60

1 constants J_{eff}^{aa} and J_{eff}^{ab} for the first two coordination spheres are positive and
2
3
4 negative, respectively, and the absolute value of J_{eff}^{aa} is more than five times
5
6
7 larger than J_{eff}^{ab} . The calculated magnetic parameters above mentioned well
8
9
10 correlate with semiconducting properties and strongly reduced both the long and
11
12 short range FM interactions of the $\text{CuCr}_{1.6}\text{V}_{0.4}\text{Se}_4$ spinel. For comparison, the
13
14 relevant calculated magnetic parameters [13] of the parent CuCr_2Se_4 metallic
15
16 ferromagnet [5] are collected in Table 3.
17
18
19
20
21
22
23

24 5. Conclusions

25
26
27
28
29 We have shown that in ferromagnetic semiconductor $\text{CuCr}_{1.6}\text{V}_{0.4}\text{Se}_4$,
30 exhibiting high electrical conductivity the magnon excitations are connected
31
32 with a double exchange mechanism existing apart from the superexchange
33
34 interaction, like it was observed in the ferromagnetic spinel systems:
35
36 $\text{Zn}_x\text{Cu}_y\text{Cr}_z\text{Se}_4$ for $y \geq 0.8$ [11], $\text{Cu}_x\text{Ga}_y\text{Cr}_z\text{Se}_4$ for $0.036 \leq y \leq 0.394$ [12],
37
38 $\text{Cu}_x\text{Co}_y\text{Cr}_z\text{Se}_4$ for $0.06 \leq y \leq 0.11$ [13], and indicated by de Gennes in
39
40 manganites [35]. For comparison, in the $\text{CdCr}_{2-x}\text{Ga}_x\text{Se}_4$ spinel system [10], the
41
42 ferromagnetic coupling, being caused only by the superexchange mechanism,
43
44 does not contribute to the spin wave excitations. The big value of ESR linewidth
45
46 of $\text{CuCr}_{1.6}\text{V}_{0.4}\text{Se}_4$ and its strong temperature increase in PM state suggest the
47
48 weakly exchange-coupled Cr-Cr pairs to the lattice in comparison with the fast-
49
50 relaxing V^{3+} ions. The spin-phonon coupling is explained as the several-stage
51
52 relaxation process in which the V^{3+} ions, the exchange subsystem and
53
54
55
56
57
58
59
60

1 conduction electrons subsystem act as the intermediate reservoirs.

2
3 Our results mean that in the mixed Cr valence band with a narrow
4 bandwidth of 0.11 eV a coherent transfer of the magnon momentum to the
5 electron gas results in the negative magnetoresistance effect in the single crystal
6 under study.
7
8
9
10
11
12
13
14
15
16

17 **Acknowledgments**

18
19 This work was partly supported by Ministry of Science (Poland) and
20 funded from science resources for years 2007-2009 as a research project (Project
21 No. N N204 178433). We are indebted to the European Community for the
22 UPGOW fellowship awarded to S. Mazur for the year 2008-09.
23
24
25
26
27
28
29
30
31
32
33

34 **Appendix A**

35
36 The Debye temperature [36], θ_D , has been estimated from the following
37 formula:
38
39

$$40 \theta_D = \frac{h\nu}{2k} \sqrt[3]{\frac{6\pi^2 N}{V}} \quad (A1)$$

41
42 where h is the Planck constant, k is the Boltzmann constant, $N = 56$ is the
43 number of atoms in the spinel unit cell, $V (= a^3$, where a is the lattice parameter)
44 is the volume of the spinel unit cell and $\nu = 809$ m/s is the sound speed in the
45 CuCr₂Se₄ spinel calculated from Eq. (A1) and based on the value of $\theta_D = 280$ K
46 estimated from the heat capacity measurements and the Grüneisen constant.³⁷
47
48
49
50
51
52
53
54
55
56
57
58
59
60

We assumed the same value of the sound speed in the CuCr_{1.6}V_{0.4}Se₄ spinel and

the calculated value of θ_D for this spinel is of the same order as for the CuCr_2Se_4 one (see Table 2).

Appendix B

To determine the exchange constants of the superexchange and double exchange interactions an estimation of the Cr^{3+} and Cr^{4+} portions is necessary. Portions x_3 and x_4 of the chromium ions: Cr^{3+} and Cr^{4+} , respectively, were calculated from the saturation magnetization M_s :

$$M_s = 2(g_3 S_3 x_3 + g_4 S_4 x_4 + g_4 S_4 x) \quad (\text{B1})$$

taking into account the following normalization condition: $x_3 + x_4 + x = 1$, where $M_s = 4.66 \mu_B$ is the experimental value of the saturation magnetization, $S_3 = 3/2$ is the spin of Cr^{3+} ion, $S_4 = 1$ is the spin of Cr^{4+} and V^{3+} ions, $g_3 = 2.0$ and $g_4 = 1.86$ are the Landé factors for Cr^{3+} , Cr^{4+} and V^{3+} ions, respectively, and $x = 0.2$ is the normalized content of V^{3+} ions.

The exchange constants of superexchange and double exchange interactions between the first two coordination spheres were calculated using the exchange Hamiltonian as follows:

$$H = H_{se} + H_{de} \quad (\text{B2})$$

where:

$$H_{se} = -\sum_{\substack{i,j \\ i \neq j}} J_{ij} \vec{S}_i \cdot \vec{S}_j, \quad (\text{B3})$$

represents the superexchange Cr^{n+} -Se- Cr^{m+} and Cr^{m+} -Se-Se- Cr^{n+} interactions [4] with the integrals J_{ij} and $c_{aa} = 6$ and $c_{ab} = 12$ numbers of nearest neighbours in

the first and second Cr-Cr coordination spheres, respectively. The spins \vec{S}_i and \vec{S}_j are considered as the quasiclassical vectors.

$$H_{de} = -\frac{1}{6}x_3x_4 \sum_{\substack{i,j \\ i \neq j}} b_{ij} \vec{S}_i \cdot \vec{S}_j, \quad (\text{B4})$$

represents the double exchange interactions [4] with x_3 and x_4 being the concentration of Cr^{3+} and Cr^{4+} ions, which is normalized in such way that $x_3 + x_4 + x = 1$ as from the ESR studies it follows that V^{3+} ions are directly coupled to the lattice, and b_{ij} is the hopping integral between the atomic t_{2g} states $|i\rangle$ and $|j\rangle$ for neighbours $\langle i,j \rangle$. We take the band factor as $\sim x_3x_4$ corresponding to probability of finding one atom in the state Cr^{3+} and the neighbouring one in the state Cr^{4+} . The number 1/6 in the double exchange Hamiltonian (B4) is a constant of a bilinear term $\vec{S}_i \cdot \vec{S}_j$ in the case of spin 1 [38]. Additionally, we take the hopping electron between two Cr ions on the same footing as the remaining ones. Because all t_{2g} electrons are quantum mechanically indistinguishable, the Cr cations supply both localized and itinerant $3d$ moments when Cr^{4+} cations are present [4].

According to the Hamiltonian (B2) the effective exchange constants [4] for the first two coordination spheres are:

$$J_{eff}^{aa} = J_{aa}c_{aa} + \frac{1}{6}b_{aa}c_{aa}x_3x_4, \quad (\text{B5})$$

$$J_{eff}^{ab} = J_{ab}c_{ab} + \frac{1}{6}b_{ab}c_{ab}x_3x_4. \quad (\text{B6})$$

The J_{aa} and b_{aa} and J_{ab} and b_{ab} integrals for the first two coordination spheres, respectively, are calculated from the high temperature expansion of the magnetic susceptibility [4]. These calculations are based on the equations describing the

1 contributions to the paramagnetic Curie-Weiss temperature resulting from the
 2
 3 separate mechanisms of the superexchange and double exchange interactions as
 4
 5 follows [39]:
 6
 7

$$9 \quad \theta_{CW} = \theta_{se} + \theta_{de} \quad (B7)$$

10 where θ_{CW} is the paramagnetic Curie-Weiss temperature (from experiment), θ_{se}
 11
 12 is the superexchange contribution to θ_{CW} and θ_{de} is the double exchange
 13
 14 contribution to θ_{CW} . The above contributions [4,39] can be read:
 15
 16
 17

$$18 \quad \theta_{se} = \frac{2}{3} X \sum_p J_p c_p, \quad (B8)$$

$$19 \quad \theta_{de} = \frac{1}{6} X x_3 x_4 \sum_p b_p c_p, \quad (B9)$$

20 where $\sum_p J_p c_p = \theta_{Cu}$ was taken from Ref. 4 and equal to 90 K for the CuCr_2Se_4
 21
 22
 23
 24
 25
 26
 27
 28
 29
 30
 31
 32
 33
 34
 35
 36
 37
 38
 39
 40
 41
 42
 43
 44
 45
 46
 47
 48
 49
 50
 51
 52
 53
 54
 55
 56
 57
 58
 59
 60
 61
 62
 63
 64
 65
 66
 67
 68
 69
 70
 71
 72
 73
 74
 75
 76
 77
 78
 79
 80
 81
 82
 83
 84
 85
 86
 87
 88
 89
 90
 91
 92
 93
 94
 95
 96
 97
 98
 99
 100
 101
 102
 103
 104
 105
 106
 107
 108
 109
 110
 111
 112
 113
 114
 115
 116
 117
 118
 119
 120
 121
 122
 123
 124
 125
 126
 127
 128
 129
 130
 131
 132
 133
 134
 135
 136
 137
 138
 139
 140
 141
 142
 143
 144
 145
 146
 147
 148
 149
 150
 151
 152
 153
 154
 155
 156
 157
 158
 159
 160
 161
 162
 163
 164
 165
 166
 167
 168
 169
 170
 171
 172
 173
 174
 175
 176
 177
 178
 179
 180
 181
 182
 183
 184
 185
 186
 187
 188
 189
 190
 191
 192
 193
 194
 195
 196
 197
 198
 199
 200
 201
 202
 203
 204
 205
 206
 207
 208
 209
 210
 211
 212
 213
 214
 215
 216
 217
 218
 219
 220
 221
 222
 223
 224
 225
 226
 227
 228
 229
 230
 231
 232
 233
 234
 235
 236
 237
 238
 239
 240
 241
 242
 243
 244
 245
 246
 247
 248
 249
 250
 251
 252
 253
 254
 255
 256
 257
 258
 259
 260
 261
 262
 263
 264
 265
 266
 267
 268
 269
 270
 271
 272
 273
 274
 275
 276
 277
 278
 279
 280
 281
 282
 283
 284
 285
 286
 287
 288
 289
 290
 291
 292
 293
 294
 295
 296
 297
 298
 299
 300
 301
 302
 303
 304
 305
 306
 307
 308
 309
 310
 311
 312
 313
 314
 315
 316
 317
 318
 319
 320
 321
 322
 323
 324
 325
 326
 327
 328
 329
 330
 331
 332
 333
 334
 335
 336
 337
 338
 339
 340
 341
 342
 343
 344
 345
 346
 347
 348
 349
 350
 351
 352
 353
 354
 355
 356
 357
 358
 359
 360
 361
 362
 363
 364
 365
 366
 367
 368
 369
 370
 371
 372
 373
 374
 375
 376
 377
 378
 379
 380
 381
 382
 383
 384
 385
 386
 387
 388
 389
 390
 391
 392
 393
 394
 395
 396
 397
 398
 399
 400
 401
 402
 403
 404
 405
 406
 407
 408
 409
 410
 411
 412
 413
 414
 415
 416
 417
 418
 419
 420
 421
 422
 423
 424
 425
 426
 427
 428
 429
 430
 431
 432
 433
 434
 435
 436
 437
 438
 439
 440
 441
 442
 443
 444
 445
 446
 447
 448
 449
 450
 451
 452
 453
 454
 455
 456
 457
 458
 459
 460
 461
 462
 463
 464
 465
 466
 467
 468
 469
 470
 471
 472
 473
 474
 475
 476
 477
 478
 479
 480
 481
 482
 483
 484
 485
 486
 487
 488
 489
 490
 491
 492
 493
 494
 495
 496
 497
 498
 499
 500
 501
 502
 503
 504
 505
 506
 507
 508
 509
 510
 511
 512
 513
 514
 515
 516
 517
 518
 519
 520
 521
 522
 523
 524
 525
 526
 527
 528
 529
 530
 531
 532
 533
 534
 535
 536
 537
 538
 539
 540
 541
 542
 543
 544
 545
 546
 547
 548
 549
 550
 551
 552
 553
 554
 555
 556
 557
 558
 559
 560
 561
 562
 563
 564
 565
 566
 567
 568
 569
 570
 571
 572
 573
 574
 575
 576
 577
 578
 579
 580
 581
 582
 583
 584
 585
 586
 587
 588
 589
 590
 591
 592
 593
 594
 595
 596
 597
 598
 599
 600
 601
 602
 603
 604
 605
 606
 607
 608
 609
 610
 611
 612
 613
 614
 615
 616
 617
 618
 619
 620
 621
 622
 623
 624
 625
 626
 627
 628
 629
 630
 631
 632
 633
 634
 635
 636
 637
 638
 639
 640
 641
 642
 643
 644
 645
 646
 647
 648
 649
 650
 651
 652
 653
 654
 655
 656
 657
 658
 659
 660
 661
 662
 663
 664
 665
 666
 667
 668
 669
 670
 671
 672
 673
 674
 675
 676
 677
 678
 679
 680
 681
 682
 683
 684
 685
 686
 687
 688
 689
 690
 691
 692
 693
 694
 695
 696
 697
 698
 699
 700
 701
 702
 703
 704
 705
 706
 707
 708
 709
 710
 711
 712
 713
 714
 715
 716
 717
 718
 719
 720
 721
 722
 723
 724
 725
 726
 727
 728
 729
 730
 731
 732
 733
 734
 735
 736
 737
 738
 739
 740
 741
 742
 743
 744
 745
 746
 747
 748
 749
 750
 751
 752
 753
 754
 755
 756
 757
 758
 759
 760
 761
 762
 763
 764
 765
 766
 767
 768
 769
 770
 771
 772
 773
 774
 775
 776
 777
 778
 779
 780
 781
 782
 783
 784
 785
 786
 787
 788
 789
 790
 791
 792
 793
 794
 795
 796
 797
 798
 799
 800
 801
 802
 803
 804
 805
 806
 807
 808
 809
 810
 811
 812
 813
 814
 815
 816
 817
 818
 819
 820
 821
 822
 823
 824
 825
 826
 827
 828
 829
 830
 831
 832
 833
 834
 835
 836
 837
 838
 839
 840
 841
 842
 843
 844
 845
 846
 847
 848
 849
 850
 851
 852
 853
 854
 855
 856
 857
 858
 859
 860
 861
 862
 863
 864
 865
 866
 867
 868
 869
 870
 871
 872
 873
 874
 875
 876
 877
 878
 879
 880
 881
 882
 883
 884
 885
 886
 887
 888
 889
 890
 891
 892
 893
 894
 895
 896
 897
 898
 899
 900
 901
 902
 903
 904
 905
 906
 907
 908
 909
 910
 911
 912
 913
 914
 915
 916
 917
 918
 919
 920
 921
 922
 923
 924
 925
 926
 927
 928
 929
 930
 931
 932
 933
 934
 935
 936
 937
 938
 939
 940
 941
 942
 943
 944
 945
 946
 947
 948
 949
 950
 951
 952
 953
 954
 955
 956
 957
 958
 959
 960
 961
 962
 963
 964
 965
 966
 967
 968
 969
 970
 971
 972
 973
 974
 975
 976
 977
 978
 979
 980
 981
 982
 983
 984
 985
 986
 987
 988
 989
 990
 991
 992
 993
 994
 995
 996
 997
 998
 999
 1000

$$X = x_3 S_3(S_3 + 1) + x_4 S_4(S_4 + 1) + x S_4(S_4 + 1). \quad (B10)$$

Finally, Eq. (B7) can be written:

$$\theta_{CW} = \frac{2}{3} X \theta_{Cu} + \frac{1}{6} X x_3 x_4 B, \quad (B11)$$

with the following superexchange and double exchange contributions to θ_{CW} ,
 respectively:

$$\theta_{se} = \frac{2}{3} X \theta_{Cu}, \quad (B12)$$

$$\theta_{de} = \frac{1}{6} X x_3 x_4 B. \quad (B13)$$

Eq. (B11) allows to estimate the mixed valence (Cr^{3+}, Cr^{4+}) bandwidth, W_d , of the $3d t_{2g}$ band from the relation [4]:

$$W_d = 2B. \quad (B14)$$

Using the Holland and Brown equations [40] we can calculate the superexchange integrals J_{aa} and J_{ab} for the first two coordination spheres, taking into account the estimated values of θ_{se} from Eq. (B12) and the experimental values of the Curie temperature T_C .

$$\theta_{se} = 5(3J_{aa} + 18J_{ab}), \quad (B15)$$

$$T_C = 5(J_{aa} - 2J_{ab}). \quad (B16)$$

The double exchange b_{aa} and b_{ab} integrals⁴ can be calculated from the equation:

$$B = 6b_{aa} + 36b_{ab}, \quad (B17)$$

where b_{aa} stands for the contribution from the 6 nearest neighbours and b_{ab} stands for the contributions from the 36 second nearest neighbours and from the Lotgering [5] considerations:

$$b_{aa} = 5b_{ab} \quad (B18)$$

The calculated magnetic parameters: θ_{se} , θ_{de} , B , W_d , J_{aa} , J_{ab} , J_{ab} , b_{aa} , b_{ab} , J_{eff}^{aa} , J_{eff}^{ab} are collected in Table 3.

References

- [1] J. Kanamori, J. Phys. Chem. Solids 10 (1959) p.87.
 [2] P.K. Baltzer, P.J. Wojtowicz, M. Robbins and E. Lopatin, Phys. Rev. 151

1 (1966) p.367.

2
3 [3] P.K. Baltzer, H.W. Lehmann and M. Robbins, Phys. Rev. Lett. 15 (1965)
4
5 p.493.
6
7

8
9 [4] J. Krok, J. Spalek, S. Juszczyk and J. Warczewski, Phys. Rev. B 28 (1983)
10
11 p.6499.
12
13

14 [5] F.K. Lotgering, in *Proceedings of the International Conference on*
15
16 *Magnetism, Nottingham, 1964* (Institute of Physics, London, 1965), p.533.
17
18

19 [6] F.K. Lotgering and R.P. Van Stapele, Solid State Commun. 5 (1967) p.143.
20
21

22 [7] C.Th. Hollander, G. Sawatzky and C. Haas, Solid State Commun. 15 (1974)
23
24 p.747.
25
26

27 [8] O. Yamashita, Y. Yamaguchi, I. Nakatani, H. Watanabe and K. Masumoto, J.
28
29 Phys. Soc. Japan 46 (1979) p.1145.
30
31

32 [9] M. Robbins, A. Menth, M.A. Miksovsky and R.C. Sherwood, J. Phys. Chem.
33
34 Solids 31 (1970) p.423.
35
36

37 [10] T. Groń, A. Krajewski, J. Kusz, E. Malicka, I. Okońska-Kozłowska and A.
38
39 Waškowska, Phys. Rev. B 71 (2005) p.035208.
40
41

42 [11] T. Groń, A. Krajewski, H. Duda and P. Urbanowicz, Physica B 373 (2006)
43
44 p.245.
45
46

47 [12] T. Groń, S. Mazur, H. Duda, J. Krok-Kowalski and E. Malicka, Physica B
48
49 391 (2007) p.371.
50
51

52 [13] T. Groń, S. Mazur, H. Duda, J. Krok-Kowalski and E. Maciążek, J. Alloys
53
54 Compd. 467 (2009) p.112.
55
56

57 [14] S. Mazur, T. Groń and I. Jendrzejewska, J. Alloys Compd. 480 (2009) p.19.
58
59
60

- 1 [15] N. Bloembergen and S. Wang, *Phys. Rev.* 93 (1954) p.72.
2
3
4 [16] I. Okońska-Kozłowska and J. Kopyczok, *Acta. Cryst.* C49 (1993) p.1448.
5
6 [17] *CrysAlis CCD* and *CrysAlis RED*, Oxford Diffraction Ltd., (2004)
7
8 Wrocław, Poland.
9
10
11 [18] G.M. Sheldrick, "SHELXL-99, Program for the Refinement of Crystal
12 Structures", University of Göttingen, 1997.
13
14
15 [19] C. A. Bates, A. Gavaix, P. Steggle, A. Vasson and A. M. Vasson, *J. Phys.*
16
17
18
19
20
21
22
23
24
25
26
27
28
29
30
31
32
33
34
35
36
37
38
39
40
41
42
43
44
45
46
47
48
49
50
51
52
53
54
55
56
57
58
59
60
[20] A. Bencini and D. Gatteschi, *Electron Paramagnetic Resonance of Exchange
Coupled Systems*, Springer-Verlag, Berlin Heidelberg, 1990.
[21] A. Abragam and B. Bleaney, *Electron Paramagnetic Resonance of
Transition Ions*, Clarendon Press, Oxford, 1970.
[22] S.E. Barnes, *Adv. Phys.* 30 (1981) p.801.
[23] D.L. Huber and M.S. Seehra, *J. Phys. Chem. Solids* 36 (1975) p.723.
[24] M.S. Seehra, M.M. Ibrahim, V.S. Babu and G. Srinivasan, *J. Phys.:*
Condens. Matter 8 (1996) p.11283.
[25] S.M. Bhagat and P. Lubitz, *Phys. Rev. B* 10 (1974) p.179.
[26] T. Kasuya, *Progr. Theor. Phys.* 22 (1959) p.227.
[27] H.J. Trodahl, *Phys. Rev. B* 51 (1995) p.6175.
[28] C. Kittel, *Introduction to solid state physics*, John Wiley & Sons Inc., New
York, 1966.
[29] J. Callaway, *Quantum theory of the solid state*, Academic Press, New York
and London, 1974.

- 1 [30] E. McCann and V.I. Fal'ko, J. Mag. Mag. Mater. 268 (2004) p.123.
2
3
4 [31] M. Matoba, S. Anzai and A. Fujimori, J. Phys. Soc. Jpn. 63 (1994) p.1429.
5
6
7 [32] M. Matoba, S. Anzai and A. Fujimori, J. Phys. Soc. Jpn. 60 (1991) p.4230.
8
9
10 [33] F.J. Blatt, P.A. Schroeder, C. Foiles and D. Greig, *Thermoelectric*
11
12 *power of metals*, Plenum, New York, 1976.
13
14
15 [34] N.F. Mott, *Conduction in non-crystalline materials*, Oxford Univ. Press,
16
17
18 New York, 1987.
19
20
21 [35] P.G. de Gennes, Phys. Rev. 118 (1960) p.141.
22
23
24 [36] P. Debye, Ann. Physik 39 (1912) p.789.
25
26
27 [37] Yu. Tretyakov, I.V. Gordeev and Ya.A. Kesler, J. Solid State Chem. 20
28
29 (1977) p.345.
30
31
32 [38] M. Cieplak, Phys. Rev. B 18 (1978) p.3470.
33
34
35 [39] J. Krok-Kowalski and J. Warczewski, J. Mag. Mag. Mater. 83 (1990) p.485.
36
37
38 [40] W.E. Holland and H.A. Brown, Phys. Status Solidi A 10 (1972) p.249.
39
40
41
42
43
44
45
46
47
48
49
50
51
52
53
54
55
56
57
58
59
60

Table 1. Crystal data, experimental details and structure refinement results for the $\text{CuCr}_{1.6}\text{V}_{0.4}\text{Se}_4$ single crystal.

| (I) Crystal data and experimental details | | | | | | |
|---|---|------------|------------|------------|------------------|-----------|
| Structural formula | $(\text{Cu})[\text{Cr}_{1.6}\text{V}_{0.4}]\text{Se}_4$ | | | | | |
| Space group | $Fd\bar{3}m$ (#227) | | | | | |
| Lattice parameter a (pm) | 1034.99(12) | | | | | |
| Z | 8 | | | | | |
| Calculated density d (Mg/m^3) | 5.818 | | | | | |
| Crystal size (mm×mm×mm) | 0.13×0.13×0.14 | | | | | |
| Maximum 2θ (deg) | 90.52 | | | | | |
| Index ranges: h | -13, 20 | | | | | |
| k | -20, 16 | | | | | |
| l | -20, 13 | | | | | |
| Reflections collected | 5589 | | | | | |
| Independent reflections | 262 | | | | | |
| Data/parameters | 190/10 | | | | | |
| Extinction correction | 0.0029(2) | | | | | |
| Final R indices [$I > 2\sigma(I)$]: R_1 ; wR_2 | 2.79; 6.55 | | | | | |
| Goodness of fit on F^2 | 1.009 | | | | | |
| Minimum and max $\Delta\rho$ ($\text{e}\text{\AA}^{-3}$) | -2.57; 2.86 | | | | | |
| (II) Fractional atomic coordinates and isotropic displacement parameters ($10^3 \times \text{\AA}^2$) | | | | | | |
| Atom | Site | x | y | z | U_{iso} | Occupancy |
| Cu | $8a$ | 0.125 | 0.125 | 0.125 | 9.2(1) | 1.0 |
| Cr | $16d$ | 0.5 | 0.5 | 0.5 | 10.4(2) | 0.8 |
| V | $16d$ | 0.5 | 0.5 | 0.5 | 10.4(2) | 0.2 |
| Se | $32e$ | 0.25691(3) | 0.25691(3) | 0.25691(3) | 13.99(2) | 1.0 |

(V) Selected interatomic distances (Å) and bond angles (deg)

| | |
|--|-----------|
| Cu – Se (pm) | 236.47(5) |
| Cr/V – Cu (pm) | 429.08(5) |
| Cr – Se (pm) | 251.80(3) |
| Cr – Cr (pm) | 365.92(4) |
| Se – Se shortest (pm) | 345.70(8) |
| Se – Se (pm) | 366.20(4) |
| Se – Cu – Se (deg) | 109.47(0) |
| Se – Cr/V – Se (deg) | 93.30(1) |
| Se – Cr – Se ^{<i>i</i>} (deg) | 86.70(1) |

Note: The superscript *i* denotes symmetry operator generating equivalent atom at $x+1/4$, $y+1/4$, $1-z$.

Table 2. The fitting parameters: D , E , F , G , H , I and K in Eq. (4) of the thermoelectric power analysis of the $\text{CuCr}_{1.6}\text{V}_{0.4}\text{Se}_4$ single crystal.

| D | E | F | G | H | I | K | R | θ_D |
|------------------------------|------------------------------|----------------------------|---------------|----------------------------------|----------------------------|---------------|------|------------|
| ($\mu\text{V}/\text{K}^2$) | ($\mu\text{V}/\text{K}^4$) | ($\mu\text{V}/\text{K}$) | (10^{-3}) | ($\mu\text{V}/\text{K}^{1.5}$) | ($\mu\text{V}/\text{K}$) | (10^{-3}) | % | (K) |
| 0.0227 | $1.3 \cdot 10^{-15}$ | 3.473 | 0.0054 | 0.0276 | 2.169 | 0.0071 | 99.3 | 279.7 |

R is the agreement index. The Debye temperature θ_D has been calculated from Eq. (A1).

Table 3. The calculated magnetic parameters: X , θ_{se} , θ_{de} , B , W_d , J_{aa} , J_{ab} , b_{aa} , b_{ab} , J_{eff}^{aa} and J_{eff}^{ab} of the $\text{CuCr}_{2-2x}\text{V}_{2x}\text{Se}_4$ spinel system.

| x | x_3 | x_4 | X | θ_{se} | θ_{de} | B | W_d | J_{aa} | J_{ab} | b_{aa} | b_{ab} | J_{eff}^{aa} | J_{eff}^{ab} |
|---------------------|----------------------|----------------------|-------|---------------|---------------|------|-------|----------|----------|----------|----------|----------------|----------------|
| (V^{3+}) | (Cr^{3+}) | (Cr^{4+}) | | (K) | (K) | (K) | (eV) | (K) | (K) | (K) | (K) | (K) | (K) |
| 0 | 0.512 | 0.488 | 2.896 | 90 | 340 | 4391 | 0.76 | 63.9 | -9.65 | 332.65 | 65.53 | 466.51 | -83.05 |
| 0.2 | 0.41 | 0.39 | 2.718 | 163 | 44 | 607 | 0.11 | 31.7 | -3.47 | 45.98 | 9.2 | 197.55 | -38.7 |

The values for $x = 0.0$ are taken from Ref. 13 for comparison.

Figure captions:

Figure 1. Electrical resistivity ρ and thermoelectric power S vs. temperature T .

Figure 2. Magnetoresistance $\Delta\rho/\rho_0$ vs. magnetic induction B at 4.3, 10, 15, 20 and 40 K.

Figure 3. Temperature dependences of mass susceptibility χ_σ and reciprocal mass susceptibility χ_σ^{-1} recorded at $H = 900$ Oe. The Curie temperature $T_C = 193.2$ K is indicated by arrow.

Figure 4. Mass magnetisation σ vs. magnetic field H at 4.6 K. $\sigma_s = 53.84$ Oe·cm³/g and $\mu_s = 4.66 \mu_B$ are the saturation magnetisation and saturation magnetic moment, respectively. The saturation state is marked by dashed line. Inset: the onset of the $\sigma(H)$ dependence up to 1.0 kOe.

Figure 5. The temperature dependence of the ESR parameters: (a) the resonance linewidth ΔB , (b) the resonance field B_r and (c) intensity of the spectrum DI . The Curie temperature $T_C = 193.8$ K is indicated by arrow and separates FMR and EPR resonances.

1 Figure 6. Model of paramagnetic relaxation processes of the $\text{CuCr}_{1.6}\text{V}_{0.4}\text{Se}_4$
2
3
4 spinel system.
5
6
7
8

9 Figure 7. The thermopower analysis of the $\text{CuCr}_{1.6}\text{V}_{0.4}\text{Se}_4$ spinel where S_{exp} is
10
11 the experimental curve, S_{theor} is the theoretical curve and S_{diff} , S_{ph} , S_{imp} and S_{mag}
12
13 are diffusion, phonon drag, impurity and magnon drag components of
14
15 thermopower, respectively.
16
17
18
19
20
21
22
23
24
25
26
27
28
29
30
31
32
33
34
35
36
37
38
39
40
41
42
43
44
45
46
47
48
49
50
51
52
53
54
55
56
57
58
59
60

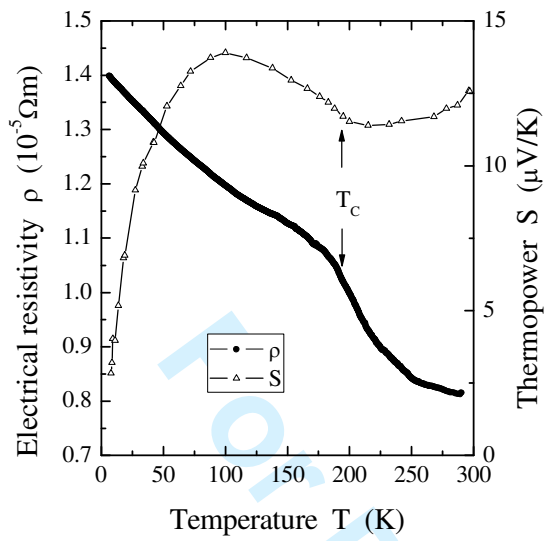


Fig.1

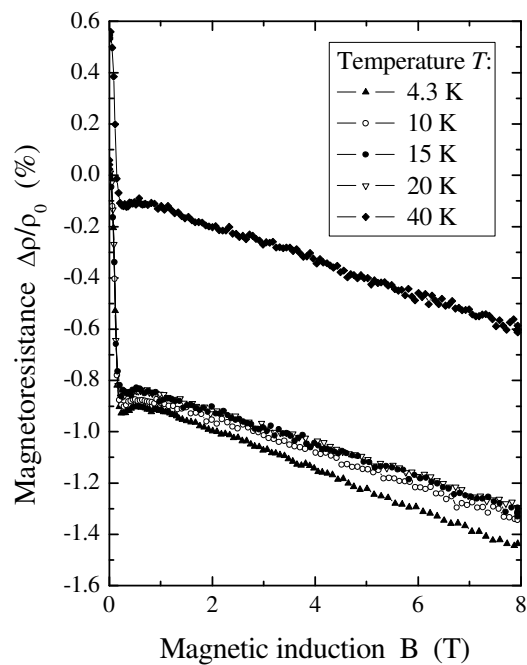


Fig.2

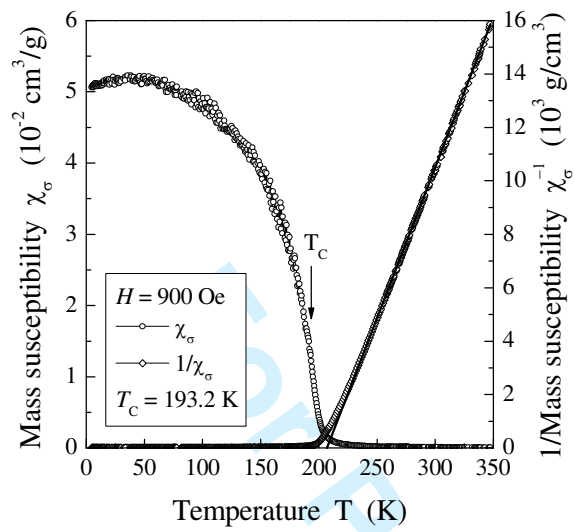


Fig.3

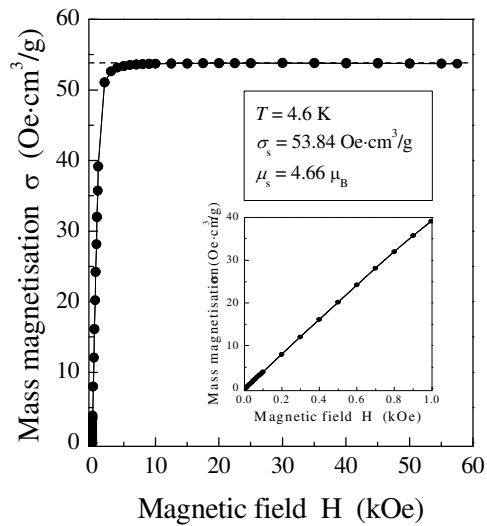


Fig.4

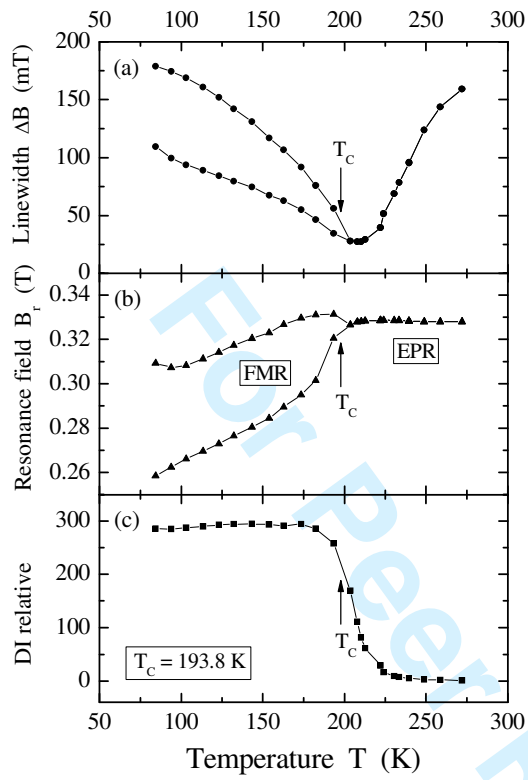


Fig.5

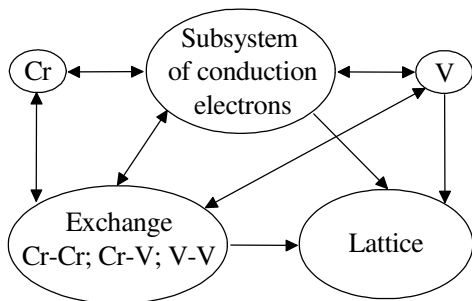


Fig.6

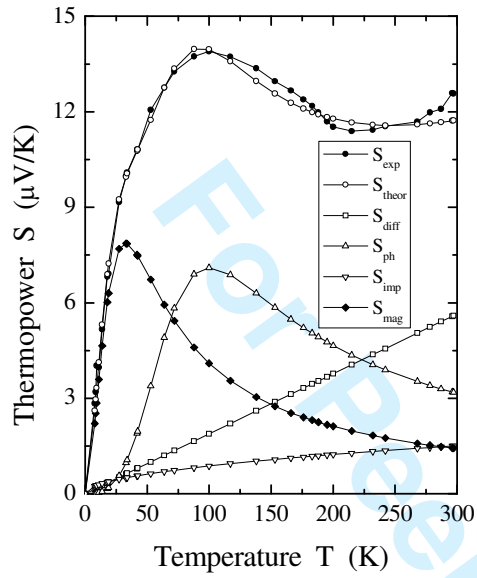


Fig.7